Supporting information for:

Free Energy of Ligand Removal in the Metal-Organic Framework UiO-66

Jessica K. Bristow,[†] Katrine Svane,[†] Davide Tiana,[†] Jonathan M. Skelton,[†]

Julian. D. Gale,[*,‡] and Aron Walsh[*,†]

†*Centre for Sustainable Chemical Technologies and Department of Chemistry, University of Bath, Claverton Down, Bath BA2 7AY, UK*

‡*Department of Applied Chemistry , Nanochemistry Research Institute, Curtin University of Technology , P.O. Box U, 6845, Perth, WA*

E-mail: j.gale@curtin.edu.au; a.walsh@bath.ac.uk

1. Substitution by monodentate ligands

When substituting a ligand for 2 monodentate molecules (one charge capping and one neutral) there is a choice on whether to do this so that the different groups are trans or cis. We identify trans to be favourable as a higher symmetry is maintained (Table S1).

Table S1: Relative energies of 1 linker removal from 2 example structures between substituting cis or trans with respect to the metal node.

System	$U_{lattice}$ cis ($kJmol^{-1}$)	$U_{lattice}$ trans ($kJmol^{-1}$)	ΔE ($kJmol^{-1}$)
Cl^-/H_2O	-216878.0	-216895.8	17.8
OH^-/H_2O	-217198.9	-217207.0	8.1

2. DMF dielectric constant

The temperature dependence of the dielectric constant as reported by Bass *et al.* was used to obtain the free energies of solvation of molecules using the COSMO program in NWChem.[S1] Table S2 gives the values extracted from reported values as published in the referenced paper. Figure S12 gives the published data points.

Table S2: Dielectric constant of DMF with temperature as reported by Bass *et al.*

Temperature (K)	Dielectric constant (ϵ_0)
215	58.0
250	47.5
300	37.2
350	29.0
400	24.0
410	23.3

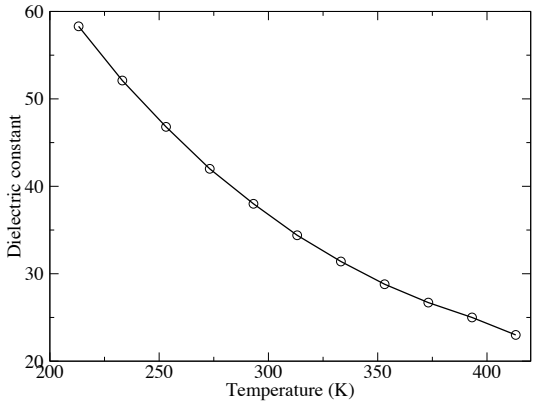

Figure S1: Dielectric constant of DMF with temperature as published by Bass *et al.*

3. Forcefield description of bulk UiO-66

Approaches to forcefield parametrisation can differ.[S2–S4] In this instance forcefield parameters are taken from CHARMM[S5,S6] with the total energy (E_{CHARMM}) calculated under the harmonic approximation considering both non-bonding and bonding parameters. We

approached the interaction between metal node and organic linker by considering these components are separate entities bonded by van der Waals and charge interactions. Organic linkers including those used for charge capping were fully described by a bonding forcefield with CHARMM parameters with Lennard-Jones non-bonding interactions. The explicit parameters will be provided in the SI. Water molecules were described with the TIP3P (original[S7] and modified[S8]) model.

$$E_{CHARMM} = \sum E^{str} + \sum E^{bnd} + \sum E^{opb} + \sum E^{tor} + \sum (E^{VdW} + E^{Coul}) \quad (1)$$

$$U^{L-J} = \frac{C_m}{\mathbf{r}^m} - \frac{C_6}{\mathbf{r}^6} \quad (2)$$

Formal charges were used for the metal ions, the head of the carboxylic acid used charges for similar carboxylic acid systems.[S9] The remaining charges were calculated in GULP[S10] using the Gasteiger charge equilibrium model considering bond increments and nearest neighbour electronegativities.[S11]

Buckingham non-bonding terms were then used to describe the interaction between metal node and organic linker to reproduce bond lengths from density functional theory (DFT):

$$U^{Buck} = Aexp(-\frac{\mathbf{r}}{\rho}) - \frac{C_6}{\mathbf{r}^6} \quad (3)$$

All Buckingham terms were fitted to recreate both structural and materials properties as previously described.

Table S3: Experiment vs. forcefield for the structural parameters of UiO-66.

Property	Experiment[S12]	forcefield
unit cell		
a	20.978	20.893
α	90.0	90.0
bond lengths		
Zr-O(carb)	2.216	2.250
Zr-O(O-H)	2.256	2.220
Zr-O(oxide)	2.062	2.083
C(carb)-O(carb)	1.275	1.279
C(benz)-C(benz)	1.389	1.376
C(benz)-C(carb)	1.491	1.507
C(benz)-H(benz)	1.094	1.083
O(O-H)-H(O-H)	0.972	0.979
bond angles		
Zr-O(oxide)-Zr	117.0	118.0
O(carb)-Zr-O(carb)	79.5	85.4
Zr-O(O-H)-Zr	102.4	107.1
O(carb)-C(carb)-O(carb)	125.9	125.0
O(carb)-C(carb)-C(benz)	117.3	117.1
C(carb)-C(benz)-C(benz)	120.0	119.7
C(benz)-C(benz)-H(benz)	121.4	121.2

4. Defect formation energies

The thermodynamic cycle considered is given in Figure S2. The description of each Gibbs free energy value used to calculate the final defect energy of formation are provided in Table S4.

Table S4: Free-energy components considered to calculate the total defect energy of formation.

Process	Description	Method of calculation
ΔG_1	desolvation of XH	NWChem
ΔG_2	gas phase dissociation of XH	NIST database
ΔG_3	defect formation energy	GULP
	(ΔG_3 = ($G_{perfect}$ + E_{XH}) - ($G_{defective}$ + E_{BDCH2}))	
ΔG_4	gas phase double protonation of BDC	NIST database
ΔG_5	solvation free-energy of BDC in DMF	NWChem

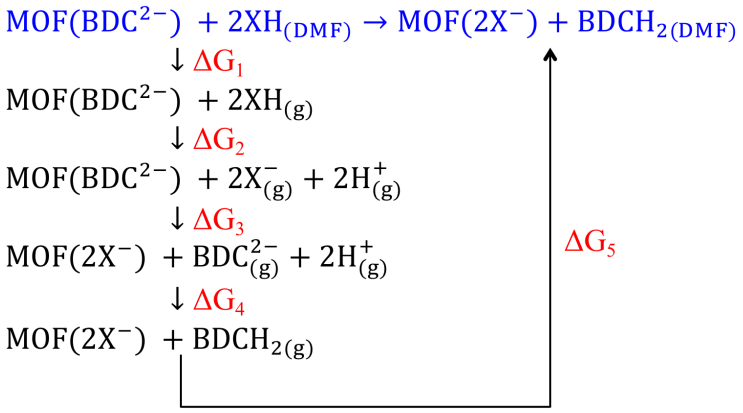

Figure S2: Thermodynamic cycle for the removal of 1 BDC linker from UiO-66, where X is the anion used for charge compensation.

Table S5: Desolvation free-energies in DMF (ΔG_1).

	Energy (kcalmol^{-1})					
Temperature (K)	215	250	300	350	400	410
HCl	3.46	3.45	3.42	3.39	3.36	3.35
H_2O	3.31	3.30	3.28	3.25	3.22	3.22
CH_3COOH	8.60	8.56	8.49	8.41	8.33	8.32
DMF	6.73	6.70	6.65	6.58	6.52	6.51

Table S6: Gas phase dissociation of X-H.

H-X	Energy (kcalmol^{-1})
HCl	328.107
H_2O	383.7
CH_3COOH	348.23

Table S7: Double protonation of BDC-H_2.

	Energy (kcalmol^{-1})
BDC-H_2	-742.09

Table S8: Solvation free-energies in DMF (ΔG_5) for BDC-H_2.

H-X	Energy (kcalmol^{-1})					
Temperature (K)	215	250	300	350	400	410
BDC-H_2	-8.05	-8.02	-7.96	-7.89	-7.82	-7.81

Table S9: Desolvation free-energies in DMF.

	Energy ($kcalmol^{-1}$)					
Temperature (K)	215	250	300	350	400	410
HCl	3.46	3.45	3.42	3.39	3.36	3.35
H_2O	3.31	3.30	3.28	3.25	3.22	3.22
CH_3COOH	8.60	8.56	8.49	8.41	8.33	8.32
DMF	6.73	6.70	6.65	6.58	6.52	6.51

5. DFT *vs.* forcefield for defective UiO-66

Table S10: Zr-ligand bond length comparison between density functional theory and our forcefield.

	Zr-Ligand bond length in Å	
Ligand	DFT/PBEsol	forcefield
Cl^-	2.536	2.505
H_2O	2.285	2.233
OH^-	2.257	2.220
DMF^-	2.279	2.284
CH_3COO^-	2.207	2.209

6. Linker vacancy configurations

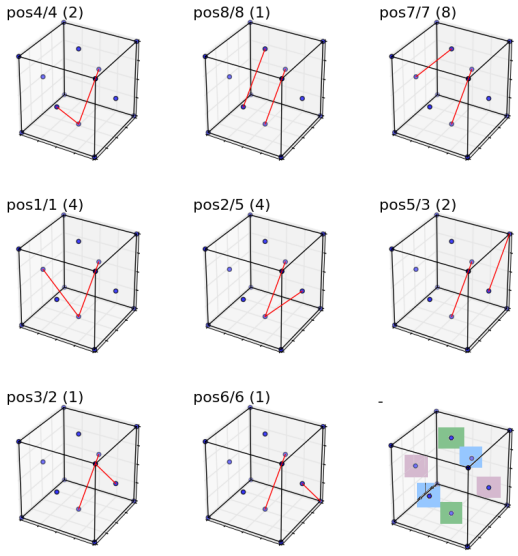

Figure S3: Configurations for 2 vacant BDC linkers. Red lines represent the missing linkers with the names of the configurations corresponding to those plotted in Figure 2 for the acetate/Cl^-/H_2O capping mechanisms, respectively. Configurations are numbered in order of defect energy magnitude and therefore differ for either capping mechanism. In brackets is the degeneracy of configuration used to calculate the Boltzmann distributions. There are 4 metal nodes in the cubic unit-cell, individual metal nodes are highlighted as green, blue and pink with all 8 corners of the plotted cubic cell making the fourth metal node.

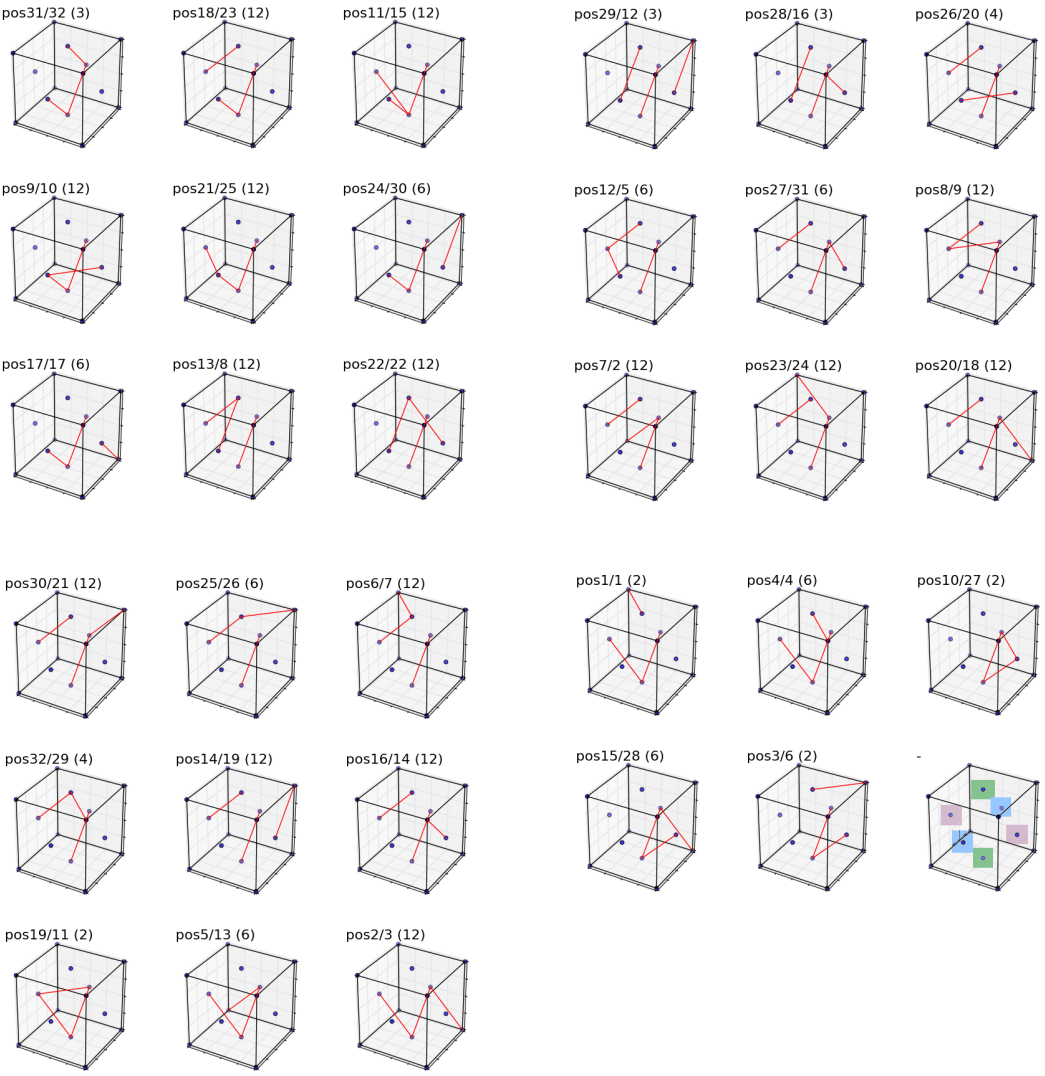

Figure S4: Configurations for 3 vacant BDC linkers. Red lines represent the missing linkers with the names of the configurations corresponding to those plotted in Figure 2 for the acetate/Cl^-/H_2O capping mechanisms respectively. Configurations are numbered in order of defect energy magnitude and therefore differ for either capping mechanism. In brackets is the degeneracy of configuration used to calculate the Boltzmann distributions. There are 4 metal nodes in the cubic unit-cell, individual metal nodes are highlighted as green, blue and pink with all 8 corners of the plotted cubic cell making the fourth metal node.

7. Free energies

Table S11: Helmholtz free energies ($kJmol^{-1}$) and overall defect formation energy (E_f(defect)) for removal of 1 linker in UiO-66 for the Cl^{-1} charge capping models. ΔA was calculated to include contributions from enthalpy and entropy for the specified temperatures ($\Delta A = \Delta U - T\Delta S$). Values given in brackets follow full volume relaxation at the stated temperature and therefore are the Gibbs free-energy ($\Delta G = \Delta H - T\Delta S$).

	Temperature (K)	A ($kJmol^{-1}$)	E_f(defect) ($kJmol^{-1}$)
Cl^-			
	215	578.2	214.5
	250	576.4	212.7
	300	574.4	210.4
	350	571.2	207.0
	400	568.6	204.1
	410	568.1	203.5
Cl^-/H_2O			
	215	470.7	134.4
	250	483.3	146.9
	300	502.0 (499.8)	165.5
	350	519.8	183.1
	400	538.4	201.4
	410	542.1	205.1
Cl^-/DMF			
	215	478.1	170.4
	250	490.0	182.0
	300	507.3	199.0
	350	523.5	214.6
	400	540.0	230.7
	410	543.3	233.8

Table S12: Helmholtz free energies (A) and overall defect formation energy (E_f(defect)) for the removal of 1 linker from UiO-66. Given in this table are results considering OH^- and CH_3COO^- charge capping models. ΔA was calculated to include contributions from enthalpy and entropy for the specified temperatures ($\Delta A = \Delta U - T\Delta S$). Values given in brackets follow full volume relaxation at the stated temperature and therefore are the Gibbs free-energy ($\Delta G = \Delta H - T\Delta S$).

	Temperature (K)	A (kJmol^{-1})	E_f(defect) (kJmol^{-1})
OH^-			
	215	166.1	293.7
	250	177.5	305.0
	300	194.2	321.7
	350	209.8	337.1
	400	225.8	352.9
	410	229.0	356.1
OH^-/H_2O			
	215	166.1	338.0
	250	177.5	349.1
	300	194.2	365.3
	350	209.8	380.3
	400	225.8	395.6
	410	229.0	398.8
OH^-/DMF			
	215	234.8	391.1
	250	246.2	401.2
	300	262.6	418.3
	350	277.6	432.7
	400	292.9	447.6
	410	295.9	450.6
CH_3COO^-			
	215	248.8	96.2
	250	256.0	103.2
	300	266.9 (265.2)	113.7
	350	276.7	123.2
	400	287.1	133.2
	410	289.2	135.3

Table S13: Overall defect formation energy per linker removal for the removal of 2 linkers from UiO-66 for the CH_3COO^{-1} charge capping models.

	E_f(defect) (kJmol^{-1})							
CH_3/OO^-								
Temperature (K)	Configuration							
	1	2	3	4	5	6	7	8
215	63.0	80.9	83.6	85.2	89.1	91.3	91.9	93.9
250	68.8	86.6	89.3	91.0	94.8	97.0	97.6	99.4
300	77.2	94.8	97.5	99.5	103.0	105.2	105.8	107.5
350	85.1	102.4	105.2	107.3	110.7	112.8	113.5	114.9
400	93.1	110.3	113.0	115.5	118.5	120.7	121.4	122.6
410	94.8	111.9	114.6	117.1	120.1	122.3	123.0	124.2
Cl^-/H_2O								
	1	2	3	4	5	6	7	8
215	115.0	129.2	129.4	130.6	132.5	132.9	133.0	133.4
250	126.3	140.6	140.8	141.7	143.9	144.3	144.4	144.8
300	142.9	157.2	157.4	157.9	160.6	160.9	161.1	161.5
350	159.0	173.3	173.5	173.5	176.8	176.9	177.2	177.6
400	175.4	189.7	189.9	189.4	193.4	193.3	193.6	194.1
410	178.7	193.0	193.2	192.6	196.7	196.5	196.9	197.4

Table S14: Overall defect formation energy per linker removal for the removal of 3 linkers from UiO-66. Given in this table are results considering CH_3COO^{-1} charge capping model.

	E_f(defect) (kJmol^{-1})							
CH_3/OO^-								
Temperature (K)	Configuration							
	1	2	3	4	5	6	7	8
215	38.1	61.9	66.2	65.5	67.3	70.2	70.5	71.4
250	43.4	67.1	71.6	70.8	72.8	75.4	75.6	76.7
300	50.9	74.5	79.3	78.5	80.8	82.8	83.0	84.3
350	58.0	81.5	86.6	85.8	88.3	89.8	90.0	91.5
400	65.3	88.6	94.0	93.1	96.0	96.9	97.1	98.7
410	66.7	90.0	95.5	94.6	97.6	98.4	98.5	100.2
	9	10	11	12	13	14	15	16
215	72.1	73.0	74.4	74.6	75.0	76.9	76.9	77.1
250	77.3	78.3	79.6	79.9	80.4	82.2	82.2	82.5
300	84.9	85.8	87.1	87.4	88.2	89.8	89.8	90.4
350	92.1	92.9	94.1	94.4	95.5	97.0	97.0	97.8
400	99.3	100.1	101.2	101.6	103.0	104.3	104.3	105.3
410	100.8	101.6	102.6	103.1	104.5	105.8	105.7	106.9
	17	18	19	20	21	22	23	24
215	80.7	81.0	81.7	82.1	82.4	82.4	82.7	83.8
250	86.2	86.4	86.9	87.3	87.6	87.7	88.1	89.1
300	94.0	94.1	94.4	94.8	95.2	95.4	96.0	96.7
350	101.3	101.3	101.5	101.8	102.3	102.6	103.4	103.8
400	108.8	108.7	108.6	109.0	109.5	110.0	110.9	111.1
410	110.3	110.2	110.1	110.4	110.9	111.5	112.5	112.6
	25	26	27	28	29	30	31	32
215	83.8	84.8	86.6	87.0	87.0	89.0	89.4	90.4
250	89.1	90.1	91.9	92.1	92.2	94.2	94.5	95.7
300	96.9	97.7	99.5	99.6	99.7	101.9	101.8	103.4
350	104.2	104.9	106.7	106.6	106.8	109.0	108.6	110.6
400	111.6	112.2	114.0	113.7	113.9	116.2	115.5	117.9
410	113.1	113.7	115.5	115.2	115.4	117.7	116.9	119.3

Table S15: Overall defect formation energy per linker removal for the removal of 3 linkers from UiO-66. Given in this table are results considering Cl^{-1}/H_2O charge capping model.

	E_f(defect) (kJmol^{-1})							
Cl^-/H_2O								
Temperature (K)	Configuration							
	1	2	3	4	5	6	7	8
215	92.4	118.8	119.4	119.9	121.1	121.5	121.7	122.1
250	103.5	129.8	130.4	130.9	132.2	132.5	132.8	133.1
300	119.7	145.8	146.4	146.9	148.1	148.3	148.8	149.0
350	135.6	161.3	162.0	162.5	163.7	163.8	164.5	164.5
400	151.7	177.1	177.9	178.3	179.6	179.6	180.4	180.3
410	155.0	180.3	181.1	181.5	182.7	182.7	183.6	183.5
	9	10	11	12	13	14	15	16
215	122.6	124.1	124.4	126.7	127.5	129.4	129.4	129.4
250	133.7	134.8	135.7	137.8	138.5	140.4	140.4	140.4
300	149.7	150.3	151.9	153.7	154.5	156.4	156.2	156.4
350	165.4	165.5	167.9	169.3	170.1	172.0	171.8	171.9
400	181.2	180.9	184.1	185.0	185.9	187.8	187.5	187.6
410	184.4	183.9	187.3	188.2	189.1	191.0	190.7	190.8
	17	18	19	20	21	22	23	24
215	129.9	130.5	130.6	131.3	131.5	131.7	132.03	132.2
250	140.9	141.6	141.7	142.4	142.5	142.8	143.00	143.2
300	156.7	157.6	157.7	158.4	158.5	158.8	158.83	159.1
350	172.1	173.3	173.4	174.0	174.1	174.5	174.30	174.7
400	187.8	189.1	189.3	189.8	189.9	190.4	189.97	190.5
410	190.9	192.3	192.4	193.0	193.1	193.6	193.10	193.7
	25	26	27	28	29	30	31	32
215	132.6	132.7	133.4	133.7	134.2	134.53	135.0	138.6
250	143.3	143.8	144.6	144.8	145.3	145.61	145.8	149.6
300	158.9	159.8	160.7	160.8	161.3	161.61	161.3	165.5
350	174.1	175.5	176.6	176.5	176.9	177.26	176.4	181.1
400	189.5	191.4	192.6	192.5	192.8	193.11	191.8	196.9
410	192.5	194.6	195.8	195.6	196.0	196.28	194.9	200.0

8. XRD for Cl^-/H_2O charge compensation

Simulated XRD patterns ($\lambda = 1.5418$ nm) for the cubic and monoclinic phases of UiO-66 calculated with 1 and 7 linkers missing are given (Figures S5 and S6).

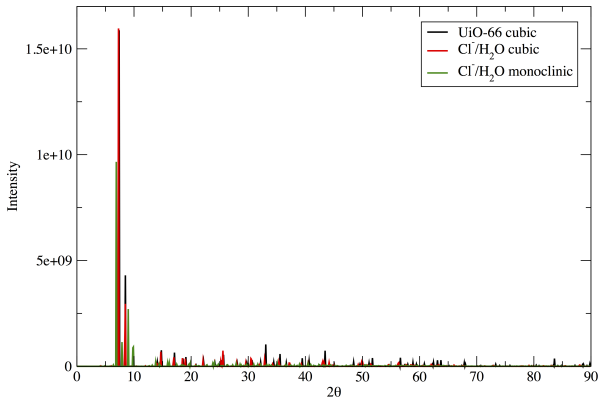

Figure S5: XRD patterns of the cubic phase of UiO-66 with 1 (black) missing linker and monoclinic phase 7 (red) missing linkers with Cl^-/H_2O as the charge capping mechanism.

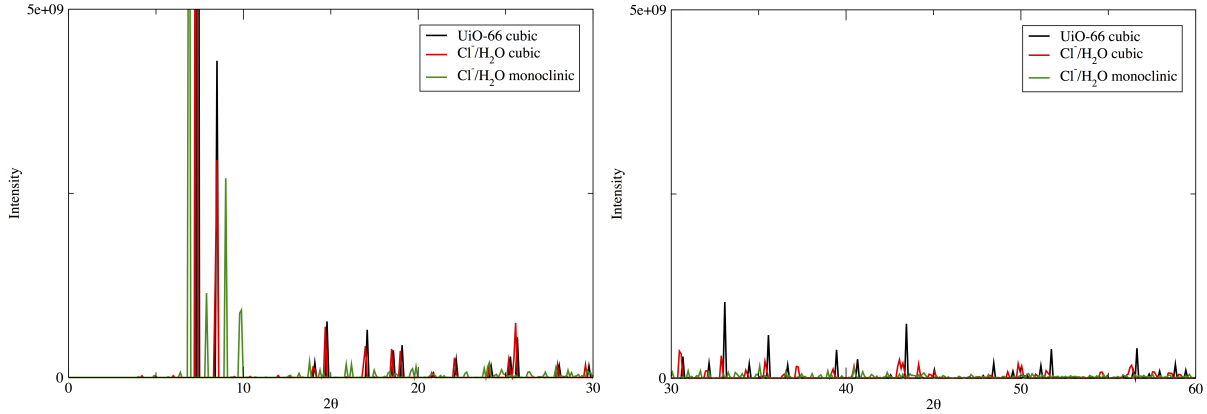

Figure S6: Zoomed in view of the XRD patterns of the cubic phase of UiO-66 with 1 (black) missing linker and monoclinic phase 7 (red) missing linkers with Cl^-/H_2O as the charge capping mechanism.

9. Vibrational and Raman spectra

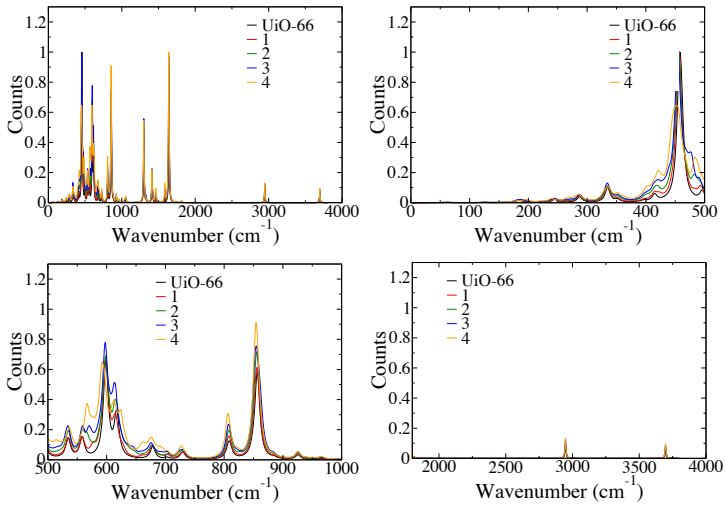

Figure S7: IR spectra of non-defective UiO-66 with 1–4 linkers removed with acetic acid capping.

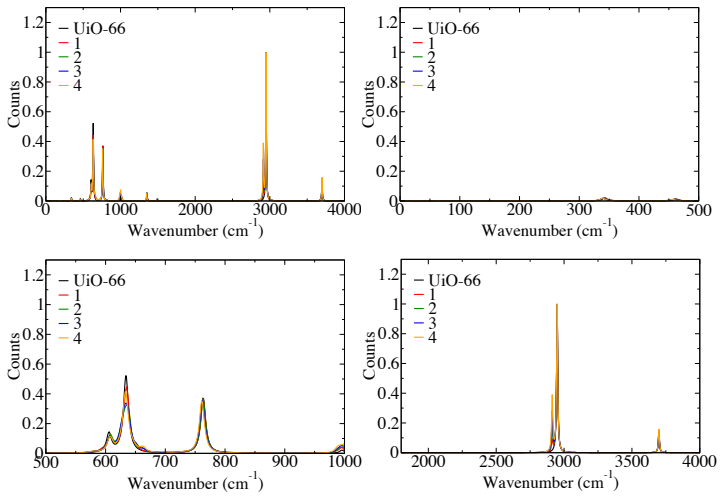

Figure S8: Raman spectra of non-defective UiO-66 with 1–4 linkers removed with acetic acid capping.

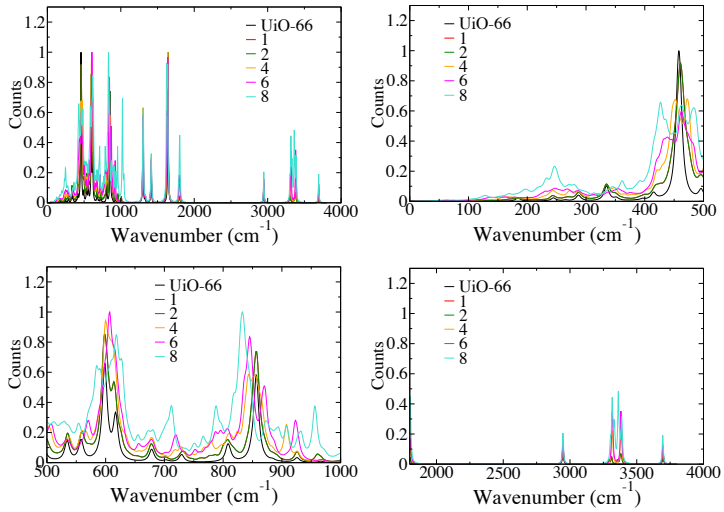

Figure S9: IR spectra of non-defective UiO-66 with 1, 2, 4, 6 and 8 linkers removed with Cl^-/H_2O capping.

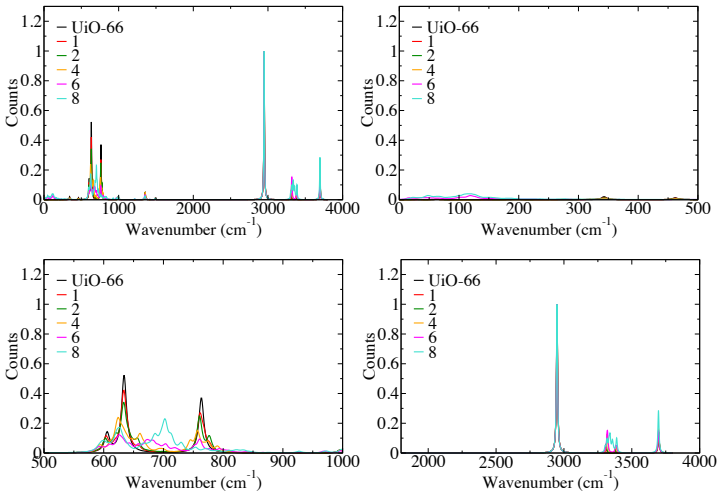

Figure S10: Raman spectra of non-defective UiO-66 with with 1, 2, 4, 6 and 8 linkers removed with Cl^-/H_2O capping.

10. Boltzmann distributions

The equilibrium distributions of defects in the structure can be estimated from

$$C_n = g_n exp(\frac{-\Delta G_n}{k_B T})/Z$$

where g_n is the degeneracy of each configuration, ΔG_n is the defect free energy (Tables S12, S13, and S14), and Z is the vibration partition function

$$Z = \sum_n g_n exp(\frac{-\Delta G_n}{k_B T})$$

Table S16: Degeneracies of defect configurations and Boltzmann population (in %) of the acetate capping for 2 linker vacancies.

Configuration	g_i	Temperature (K)					
		215	250	300	350	400	410
1	4	100.0	100.0	99.9	99.7	99.2	99.1
2	4	0.0	0.0	0.1	0.3	0.6	0.7
3	1	0.0	0.0	0.0	0.0	0.1	0.1
4	2	0.0	0.0	0.0	0.0	0.1	0.1
5	2	0.0	0.0	0.0	0.0	0.0	0.0
6	1	0.0	0.0	0.0	0.0	0.0	0.0
7	8	0.0	0.0	0.0	0.0	0.0	0.1
8	1	0.0	0.0	0.0	0.0	0.0	0.0

Table S17: Degeneracies of defect configurations and Boltzmann population (in %) of the Cl^-/H_2 capping for 2 linker vacancies.

Configuration	g_i	Temperature (K)					
		215	250	300	350	400	410
1	4	100.0	99.9	99.4	98.2	96.5	96.1
2	4	0.0	0.1	0.3	0.7	1.3	1.5
3	1	0.0	0.0	0.1	0.2	0.3	0.3
4	2	0.0	0.0	0.1	0.3	0.7	0.8
5	2	0.0	0.0	0.0	0.1	0.2	0.2
6	1	0.0	0.0	0.0	0.1	0.1	0.1
7	8	0.0	0.0	0.1	0.4	0.8	0.9
8	1	0.0	0.0	0.0	0.0	0.1	0.1

Table S18: Degeneracies of defect configurations and Boltzmann population (in %) of the acetate capping for 3 linker vacancies with temperature.

Configuration	g_i	Temperature (K)					
		215	250	300	350	400	410
1	2	100.0	100.0	100.0	99.8	99.3	99.0
2	9	0.0	0.0	0.0	0.2	0.5	0.6
3	2	0.0	0.0	0.0	0.0	0.1	0.1
4	6	0.0	0.0	0.0	0.0	0.1	0.1
5	6	0.0	0.0	0.0	0.0	0.0	0.0
6	12	0.0	0.0	0.0	0.0	0.0	0.1
7	12	0.0	0.0	0.0	0.0	0.0	0.1
8	12	0.0	0.0	0.0	0.0	0.0	0.0
9	12	0.0	0.0	0.0	0.0	0.0	0.0
10	2	0.0	0.0	0.0	0.0	0.0	0.0
11	12	0.0	0.0	0.0	0.0	0.0	0.0
12	4	0.0	0.0	0.0	0.0	0.0	0.0
13	12	0.0	0.0	0.0	0.0	0.0	0.0
14	12	0.0	0.0	0.0	0.0	0.0	0.0
15	6	0.0	0.0	0.0	0.0	0.0	0.0
16	12	0.0	0.0	0.0	0.0	0.0	0.0
17	6	0.0	0.0	0.0	0.0	0.0	0.0
18	12	0.0	0.0	0.0	0.0	0.0	0.0
19	2	0.0	0.0	0.0	0.0	0.0	0.0
20	8	0.0	0.0	0.0	0.0	0.0	0.0
21	12	0.0	0.0	0.0	0.0	0.0	0.0
22	12	0.0	0.0	0.0	0.0	0.0	0.0
23	4	0.0	0.0	0.0	0.0	0.0	0.0
24	6	0.0	0.0	0.0	0.0	0.0	0.0
25	6	0.0	0.0	0.0	0.0	0.0	0.0
26	4	0.0	0.0	0.0	0.0	0.0	0.0
27	6	0.0	0.0	0.0	0.0	0.0	0.0
28	3	0.0	0.0	0.0	0.0	0.0	0.0
29	3	0.0	0.0	0.0	0.0	0.0	0.0
30	12	0.0	0.0	0.0	0.0	0.0	0.0
31	3	0.0	0.0	0.0	0.0	0.0	0.0
32	4	0.0	0.0	0.0	0.0	0.0	0.0

Table S19: Degeneracies of defect configurations and Boltzmann population (in %) of the Cl^-/H_2O capping for 3 linker vacancies with temperature.

Configuration	g_i	Temperature (K)					
		215	250	300	350	400	410
1	2	100.0	100.0	100.0	99.8	98.9	98.7
2	12	0.0	0.0	0.0	0.1	0.3	0.4
3	2	0.0	0.0	0.0	0.1	0.2	0.3
4	6	0.0	0.0	0.0	0.0	0.1	0.1
5	6	0.0	0.0	0.0	0.0	0.1	0.1
6	12	0.0	0.0	0.0	0.0	0.0	0.0
7	12	0.0	0.0	0.0	0.0	0.1	0.1
8	12	0.0	0.0	0.0	0.0	0.1	0.1
9	12	0.0	0.0	0.0	0.0	0.1	0.1
10	2	0.0	0.0	0.0	0.0	0.1	0.1
11	12	0.0	0.0	0.0	0.0	0.0	0.0
12	2	0.0	0.0	0.0	0.0	0.0	0.0
13	12	0.0	0.0	0.0	0.0	0.0	0.0
14	12	0.0	0.0	0.0	0.0	0.0	0.0
15	12	0.0	0.0	0.0	0.0	0.0	0.0
16	6	0.0	0.0	0.0	0.0	0.0	0.0
17	6	0.0	0.0	0.0	0.0	0.0	0.0
18	12	0.0	0.0	0.0	0.0	0.0	0.0
19	2	0.0	0.0	0.0	0.0	0.0	0.0
20	12	0.0	0.0	0.0	0.0	0.0	0.0
21	12	0.0	0.0	0.0	0.0	0.0	0.0
22	12	0.0	0.0	0.0	0.0	0.0	0.0
23	4	0.0	0.0	0.0	0.0	0.0	0.0
24	6	0.0	0.0	0.0	0.0	0.0	0.0
25	6	0.0	0.0	0.0	0.0	0.0	0.0
26	4	0.0	0.0	0.0	0.0	0.0	0.0
27	6	0.0	0.0	0.0	0.0	0.0	0.0
28	3	0.0	0.0	0.0	0.0	0.0	0.0
29	3	0.0	0.0	0.0	0.0	0.0	0.0
30	12	0.0	0.0	0.0	0.0	0.0	0.0
31	3	0.0	0.0	0.0	0.0	0.0	0.0
32	4	0.0	0.0	0.0	0.0	0.0	0.0

11. Multiple vacancies with OH^-/H_2O capping

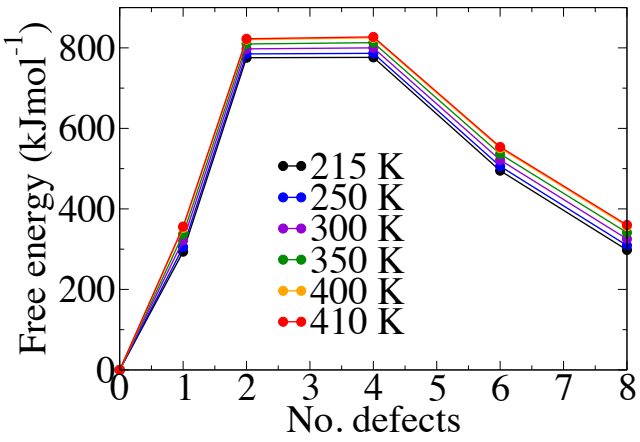

Figure S11: Reaction energy for removing 1–8 linkers from UiO-66 with OH^-/H_2O capping. NU-1000 is UiO-66 with 8 linkers missing. The path for linker removal was chosen to maintain the highest symmetry to reach NU-1000 topology.

12. Forcefield parameters and atom types

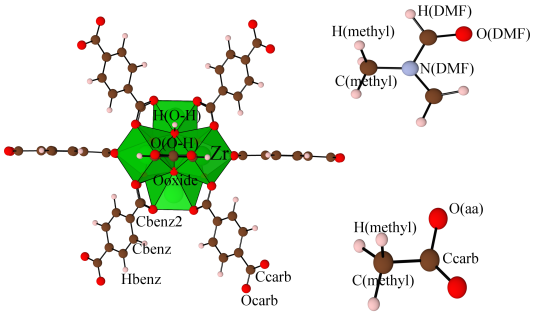

Figure S12: Atom types used for UiO-66 framework and charge compensating molecules.

Table S20: Charges used for the UiO-66 framework. Atom types are given in Figure S9.

atom type	charge
H(O-H)	0.15
Hbenz	0.11
Cbenz	-0.07
Cbenz2	0.01
Ccarb	1.17
Ocarb	-1.13
Ooxide	-2.00
O(OH)	-1.15
Zr	4.00

Table S21: Non-bonding parameters for the UiO-66 framework. Note the absence of Lennard-Jones parameters for Zr and O(oxide) to avoid double counting of interactions associated with the metal node. Lennard-Jones total energy is calculated using epsilon/sigma rather than A and B typical constants. $E_{L-J} = \epsilon(\sigma/\mathbf{r})^{12}$ - $2(\sigma/\mathbf{r})^{6}$. Cut-off was set to 12.5$\AA$ and 12.0$\AA$ for Lennard-Jones and Buckingham parameters, respectively.

Lennard-Jones			
atom type	epsilon (eV)	sigma (AA)	
H(O-H)	0.130E-02	1.358	
Hbenz	0.130E-02	1.358	
Cbenz	0.304E-02	1.992	
Cbenz2	0.304E-02	1.992	
Ccarb	0.304E-02	2.000	
Ocarb	0.520E-02	1.700	
Ooxide	-	-	
O(OH)	0.833E-02	1.765	
Zr	-	-	
Buckingham			
atom types	A (eV)	ρ (Å)	C (eVÅ^6)
Ooxide-Zr	7290.347	0.261	0.000
Ocarb-Zr	2622.296	0.297	0.000
O(O-H)-Zr	2577.933	0.297	0.000

Table S22: Bonding parameters for the UiO-66 framework.

Bond stretch			
Atom types	k (eVÅ^{-2})	$\mathbf{r}_0$	
Cbenz2-Ccarb	17.346	1.500	
Cbenz-Cbenz	26.452	1.375	
Cbenz2-Cbenz	26.452	1.375	
Hbenz-Cbenz	29.488	1.080	
Ccarb-Ocarb	45.533	1.260	
H(O-H)-O(O-H)	47.267	0.960	
Bond angles			
Atom types	k (eVrad^{-2})	θ_0	
Ccarb-Ocarb-Ocarb	8.673	133.0	
Cbenz-Cbenz2-Cbenz	3.469	120.0	
Cbenz2-Cbenz-Cbenz	3.469	120.0	
Cbenz2-Cbenz-Ccarb	3.903	119.0	
Cbenz-Hbenz-Cbenz2	2.602	120.0	
Cbenz-Hbenz-Cbenz	2.602	120.0	
Ccarb-Cbenz2-Ocarb	3.469	116.0	
Torsions			
Atom types	k (eV)	nphase	$\phi_0(^\circ)$
Cbenz2-Cbenz-Cbenz-Cbenz2	0.134	2	180.0
Cbenz-Cbenz2-Cbenz-Cbenz	0.134	2	180.0
Cbenz2-Cbenz-Cbenz-Hbenz	0.182	2	180.0
Cbenz-Cbenz2-Cbenz-Hbenz	0.182	2	180.0
Ocarb-Ccarb-Cbenz2-Cbenz	0.134	2	180.0
Ccarb-Cbenz2-Cbenz-Cbenz	0.134	2	180.0
Ccarb-Cbenz2-Cbenz-Hbenz	0.104	2	180.0
Hbenz-Cbenz-Cbenz-Hbenz	0.104	2	180.0

Table S23: Charges used for DMF. Atom types are given in Figure S9.

Atom type	charge
H(methyl)	0.01
C(methyl)	0.06
H(DMF)	0.10
C(DMF)	0.97
N(DMF)	-0.42
O(DMF)	-0.83

Table S24: Non-bonding parameters for DMF. Lennard-Jones total energy is calculated using epsilon/sigma rather than A and B typical constants. $E_{L-J} = \epsilon(\sigma/\mathbf{r})^{12}$ - $2(\sigma/\mathbf{r})^{6}$. Cut-off was set to 12.5$\mathring{A}$ and 12.0$\mathring{A}$ for Lennard-Jones and Buckingham parameters, respectively.

Lennard-Jones			
atom type	epsilon (eV)	sigma (AA)	
H(methyl)	0.195E-02	1.340	
C(methyl)	0.139E-02	2.000	
H(DMF)	0.199E-02	0.900	
C(DMF)	0.477E-02	2.000	
N(DMF)	0.867E-02	1.850	
O(DMF)	0.520E-02	1.700	
Buckingham			
atom types	A (eV)	ρ (Å)	C (eVÅ^6)
O(DMF)-Zr	1392.296	0.297	0.000
H(methyl)-H(methyl)	22.000	0.425	0.000
H(methyl)-O(DMF)	100.000	0.425	0.000
H(DMF)-O(O-H)	100.000	0.425	0.000
H(methyl)-O(O-H)	100.000	0.425	0.000
O(O-H)-O(DMF)	100.000	0.425	0.000

Table S25: Bonding parameters for DMF.

Bond stretch			
Atom types	k (eVÅ^{-2})	$\mathbf{r}_0$	
C(methyl)-N(methyl)	27.320	1.434	
H(DMF)-C(DMF)	31.266	1.100	
C(DMF)-N(methyl)	37.293	1.350	
C(DMF)-O(DMF)	45.533	1.260	
H(methyl)-C(methyl)	26.799	1.111	
C(methyl)-Ccarb	37.346	1.500	
Bond angles			
Atom types	k (eVrad^{-2})	θ_0	
N(methyl)-C(methyl)-C(DMF)	3.643	119.5	
C(DMF)-N(methyl)-O(DMF)	6.938	124.0	
C(DMF)-H(DMF)-N(methyl)	3.729	115.0	
C(methyl)-H(methyl)-N(methyl)	1.710	105.0	
C(DMF)-H(DMF)-O(DMF)	1.710	113.0	
N(methyl)-C(methyl)-C(methyl)	3.903	121.0	
C(methyl)-H(methyl)-H(methyl)	3.296	110.0	
C(methyl)-H(methyl)-Ccarb	60.710	109.5	
C(methyl)-H(methyl)-H(methyl)	3.296	110.0	
Ccarb-C(methyl)-Ocarb	3.469	116.0	
Torsions			
Atom types	k (eV)	nphase	$\phi_0(^\circ)$
O(DMF)-C(DMF)-N(methyl)-C(methyl)	0.113	2	180.0
H(DMF)-C(DMF)-N(methyl)-C(methyl)	0.113	2	180.0
H(methyl)-C(methyl)-N(methyl)-C(DMF)	0.018	3	0.0
H(methyl)-C(methyl)-N(methyl)-C(methyl)	0.018	3	0.0
Ocarb-Ccarb-C(methyl)-H(methyl)	0.108	3	0.0

Table S26: Charges used for Cl^-.

Atom type	charge
Cl	-1.00

Table S27: Non-bonding parameters for Cl^-. Lennard-Jones total energy is calculated using epsilon/sigma rather than A and B typical constants. $E_{L-J} = \epsilon(\sigma/\mathbf{r})^{12}$ - $2(\sigma/\mathbf{r})^6$. Cut-off was set to 12.5$\mathring{A}$ and 12.0$\mathring{A}$ for Lennard-Jones and Buckingham parameters, respectively.

Lennard-Jones			
atom type	epsilon (eV)	sigma (AA)	
Cl	0.833E-02	1.765	
O(O-H)-Cl	0.226E-01	3.510	
Ocarb-Cl	0.474E-02	3.310	
O(DMF)-Cl	0.274E-02	3.310	
N(DMF)-Cl	0.974E-02	3.310	
Buckingham			
atom types	A (eV)	ρ (Å)	C (eVÅ^6)
Cl-Zr	2322.933	0.321	0.000
H(methyl)-Cl	22.000	0.425	0.000
H(DMF)-Cl	50.000	0.425	0.000
Hbenz-Cl	22.000	0.425	0.000

Table S28: Charges used for acetic acid. Atom types are given in Figure S9. Note that C(methyl) and H(methyl) are the same atom types as were used for DMF.

Atom type	charge
O(aa)	-1.13
H(methyl)	0.01
C(methyl)	0.06
Ccarb	1.17

Table S29: Non-bonding parameters for acetic acid. Lennard-Jones total energy is calculated using epsilon/sigma rather than A and B typical constants. $E_{L-J} = \epsilon(\sigma/\mathbf{r})^{12}$ - $2(\sigma/\mathbf{r})^6$. Cut-off was set to 12.5$\mathring{A}$ and 12.0$\mathring{A}$ for Lennard-Jones and Buckingham parameters, respectively.

Lennard-Jones			
atom type	epsilon (eV)	sigma (AA)	
O(aa)-O(DMF)	0.416E-01	3.122	
O(O-H)-O(aa)	0.216E-01	3.122	
O(aa)-Cl	0.474E-02	3.310	
Buckingham			
atom types	A (eV)	ρ (Å)	C (eVÅ^6)
O(aa)-Zr	2322.296	0.297	0.000
Ocarb-O(aa)	100.000	0.425	0.000
H(DMF)-O(aa)	100.000	0.425	0.000

Table S30: Bonding parameters for acetic acid.

Bond stretch			
Atom types	k (eVÅ^{-2})	$\mathbf{r}_0$	
Ccarb-O(aa)	45.533	1.260	
Bond angles			
Atom types	k (eVrad^{-2})	θ_0	
Ccarb-O(aa)-O(aa)	8.673	133.0	
Ccarb-Cbenz2-O(aa)	3.469	116.0	
Ccarb-C(methyl)-O(aa)	3.469	116.0	
Ccarb-C(methyl)-H(methyl)	2.633	109.5	
Torsions			
Atom types	k (eV)	nphase	$\phi_0(^\circ)$
O(aa)-Ccarb-C(methyl)-H(methyl)	0.108	3	0.0000

Table S31: Charges used for water.

Atom type	charge
H(water)	0.417
O(water)	-0.834

Table S32: Non-bonding TIP3P and new parameters for water. Lennard-Jones total energy is calculated using epsilon/sigma rather than A and B typical constants. $E_{L-J} = \epsilon(\sigma/\mathbf{r})^{12}$ - $2(\sigma/\mathbf{r})^6$. Cut-off was set to 12.5$\AA$ and 12.0$\AA$ for Lennard-Jones and Buckingham parameters, respectively.

Lennard-Jones			
atom type	epsilon (eV)	sigma (AA)	
O(water)	0.660E-02	1.768	
H(water)	0.199E-02	0.225	
O(O-H)-O(water)	0.216E-01	3.122	
O(aa)-O(water)	0.216E-01	3.122	
Ocarb-O(water)	0.216E-01	3.122	
O(DMF)-O(water)	0.216E-01	3.122	
O(water)-O(water)	0.216E-01	3.122	
Buckingham			
atom types	A (eV)	ρ (Å)	C (eVÅ^6)
O(aa)-Zr	2322.296	0.297	0.000
Ocarb-O(aa)	100.000	0.425	0.000
H(DMF)-O(aa)	100.000	0.425	0.000

Table S33: Bonding parameters for water from the TIP3P model.

Bond stretch		
Atom types	k (eVÅ^{-2})	$\mathbf{r}_0$
H(water)-O(water)	39.028	0.957
H(water)-H(water)	0.000	1.514
Bond angles		
Atom types	k (eVrad^{-2})	θ_0
O(water)-H(water)-H(water)	4.770	104.5

13. Cluster geometries

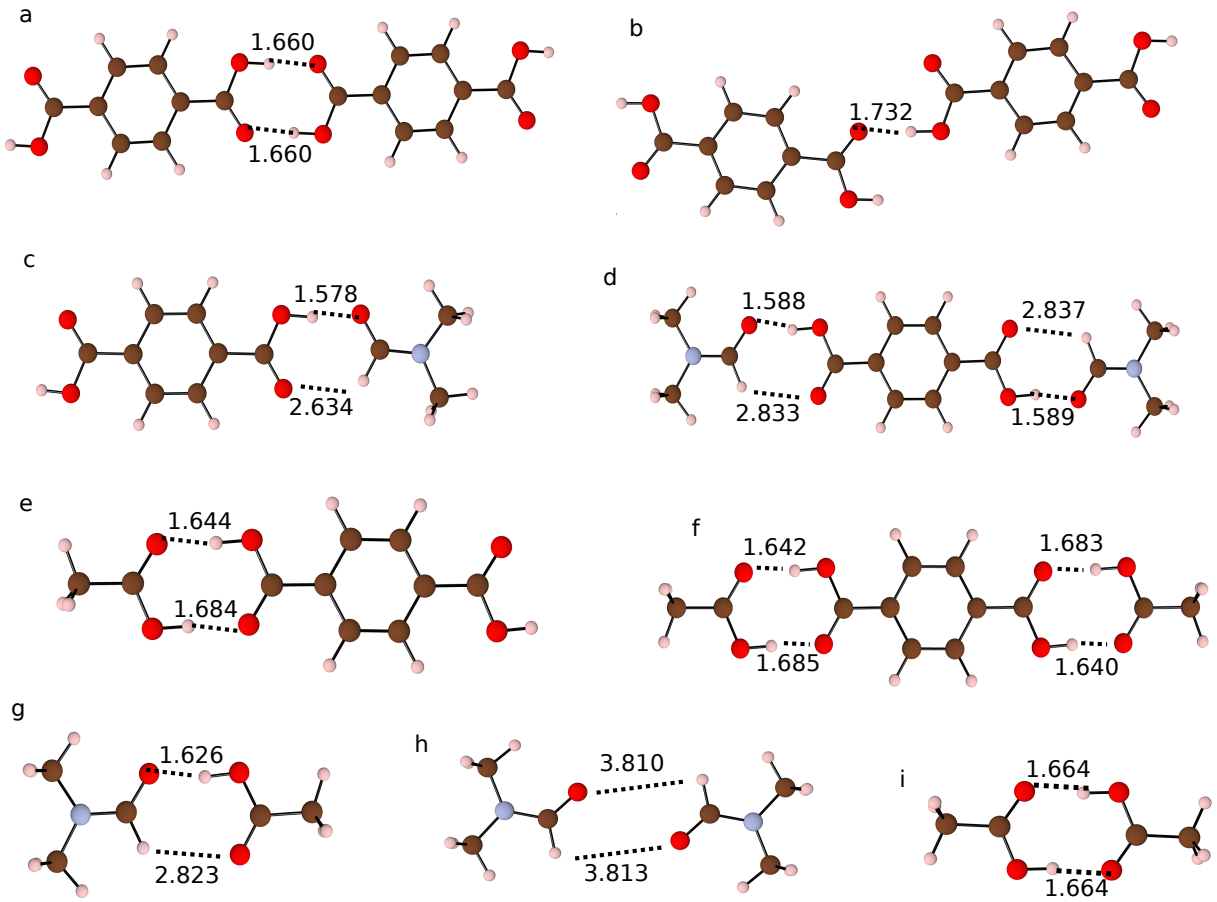

Figure S13: Measured intermolecular distances between components of clusters between molecular precursors.

References

(S1) Bass, S.; Nathan, W.; Meighan, R.; Cole, R. *J. Phys. Chem.* **1964**, *68*, 509–515.

(S2) Bristow, J. K.; Tiana, D.; Walsh, A. *J. Chem. Theory Comput.* **2014**, *10*, 4644–4652.

(S3) Addicoat, M. A.; Vankova, N.; Akter, F. I.; Heine, T. *J. Chem. Theory Comput.* **2014**, *10*, 880–891.

(S4) Bureekaew, S.; Amirjalayer, S.; Tafipolsky, M.; Spickermann, C.; Roy, T. K.; Schmid, R. *Phys. Status Solidi B* **2013**, *250*, 1128–1141.

(S5) Brooks, B. R.; Bruccoleri, R. E.; Olafson, B. D.; States, D. J.; Swaminathan, S.; Karplus, M. *J. Comput. Chem.* **1983**, *4*, 187–217.

(S6) Brooks, B. R.; Brooks, C. L.; MacKerell, A. D.; Nilsson, L.; Petrella, R. J.; Roux, B.; Won, Y.; Archontis, G.; Bartels, C.; Boresch, S. *J. Comput. Chem.* **2009**, *30*, 1545–1614.

(S7) Jorgensen, W. L.; Chandrasekhar, J.; Madura, J. D.; Impey, R. W.; Klein, M. L. *J. Chem. Phys.* **1983**, *79*, 926–935.

(S8) Neria, E.; Fischer, S.; Karplus, M. *J. Chem. Phys.* **1996**, *105*, 1902–1921.

(S9) Raiteri, P.; Demichelis, R.; Gale, J. D.; Kellermeier, M.; Gebauer, D.; Quigley, D.; Wright, L. B.; Walsh, T. R. *Farad. Discuss.* **2012**, *159*, 61–85.

(S10) Gale, J. D. *J. Chem. Soc. Faraday Trans.* **1997**, *93*, 629–637.

(S11) Gasteiger, J.; Marsili, M. *Tetrahedron* **1980**, *36*, 3219–3228.

(S12) Yang, Q.; Guillerm, V.; Ragon, F.; Wiersum, A. D.; Llewellyn, P. L.; Zhong, C.; Devic, T.; Serre, C.; Maurin, G. *Chem. Commun.* **2012**, *48*, 9831–9833.